

Real-time guidewire tracking and segmentation in intraoperative X-ray

Baochang Zhang^{a,b}, Mai Bui^{a,b}, Cheng Wang^c, Felix Bourier^{a,b}, Heribert Schunkert^{a,b,d}, and Nassir Navab^{a,e}

^aTechnical University of Munich, Germany

^bGerman Heart Center Munich, Germany

^cZhongDa Hospital Southeast University, China

^dDZHK (German Centre for Cardiovascular Research), Munich Heart Alliance, Munich, Germany

^eMunich Institute of Robotics and Machine Intelligence (MIRMI), Munich, Germany

ABSTRACT

During endovascular interventions, physicians have to perform accurate and immediate operations based on the available real-time information, such as the shape and position of guidewires observed on the fluoroscopic images, haptic information and the patients' physiological signals. For this purpose, real-time and accurate guidewire segmentation and tracking can enhance the visualization of guidewires and provide visual feedback for physicians during the intervention as well as for robot-assisted interventions. Nevertheless, this task often comes with the challenge of elongated deformable structures that present themselves with low contrast in the noisy fluoroscopic image sequences. To address these issues, a two-stage deep learning framework for real-time guidewire segmentation and tracking is proposed. In the first stage, a Yolov5s detector is trained, using the original X-ray images as well as synthetic ones, which is employed to output the bounding boxes of possible target guidewires. More importantly, a refinement module based on spatiotemporal constraints is incorporated to robustly localize the guidewire and remove false detections. In the second stage, a novel and efficient network is proposed to segment the guidewire in each detected bounding box. The network contains two major modules, namely a hessian-based enhancement embedding module and a dual self-attention module. Quantitative and qualitative evaluations on clinical intra-operative images demonstrate that the proposed approach significantly outperforms our baselines as well as the current state of the art and, in comparison, shows higher robustness to low quality images.

Keywords: Guidewire segmentation, guidewire tracking, X-ray imaging

1. INTRODUCTION

Guidewires are essential tools used in every interventional cardiology procedure. They are advanced into the cardiovascular system using percutaneous vascular access into the target area of the intervention under the guidance of real-time X-Ray fluoroscopy. Once the initial guidewire placement is successfully achieved, other catheters are advanced over the guidewires in order to provide treatments, such as stenting, ablation or drug delivery [1]. Therefore a precise navigation of the guidewire is mandatory in order to avoid damaging vascular structures, which would result in procedural complications such as perforations, dissection, stroke and hemorrhage. For this, a robust guidewire tracking and segmentation system to analyze the consecutively captured X-ray images can be of significant help and, in addition, reduce the mental workload required by the interventionist as well as prevent visual fatigue [2]. Moreover, such a system can provide visual feedback of the guidewire to robotic systems, paving the road for semi- or fully automatic robot-assisted interventions.

Further author information: (Send correspondence to Baochang Zhang)

Baochang Zhang: E-mail: baochang.zhang@tum.de

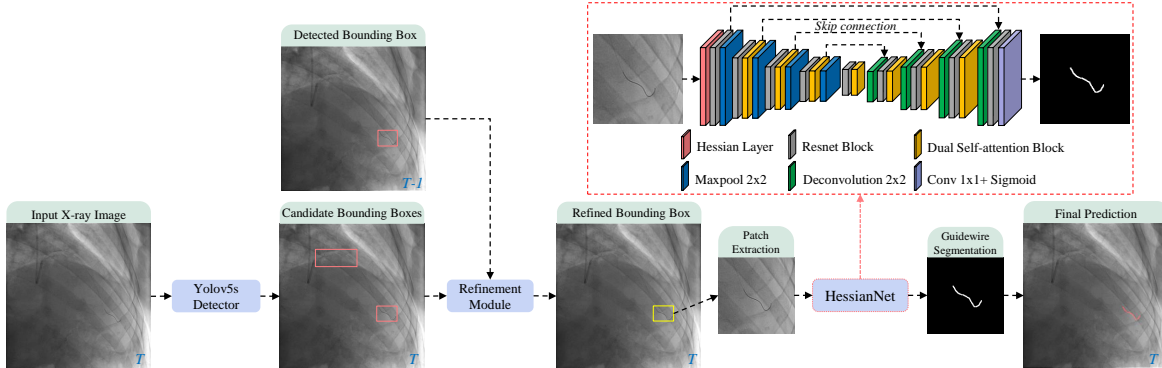


Figure 1. Our framework consists of two stages. First, the guidewire is detected in the current image frame at time step T by including temporal information and the detection of the previous frame at time step $T - 1$. Second, the guidewire is segmented in the predicted bounding box by our proposed HessianNet, which, in addition to the image information, utilizes Hessian-based features for improved guidewire segmentation.

However, due to the following reasons, guidewire segmentation and tracking still remains a challenging task: (a) guidewires present themselves as elongated deformable structures with low contrast in noisy X-ray fluoroscopy images; (b) only a small part of the guidewire is visible in the image, i.e. only a 3cm part of the guidewire contains radiopaque material and (c) their visual appearance easily resembles other anatomical structures (such as rib outlines or small vessels) in the fluoroscopic images.

Nowadays, most researchers define this task directly as a segmentation task to extract the guidewire from individual X-ray images. In general, resulting methods can be divided into traditional methods and deep learning-based methods. For traditional methods, the guidewire is extracted based on primitive features such as texture, a histogram or pixel intensity values. Meanwhile, these methods rely on manual annotation of the guidewire in the first frame of the fluoroscopic video sequence and the guidewire between two consecutive frames should not be significantly deformed [3]. In [4], segment-like features (SEGlets) were introduced to overcome large deformations between successive frames. However, hand-crafted features tend to have poor generalization capabilities and robustness, especially in noisy environments. Recently, deep learning has achieved promising results in medical image analysis. In [5, 6], instead of segmenting the guidewire directly [7, 8], a detector is deployed first to output the bounding box of the guidewire, which could reduce the class imbalance of the segmentation task. However, these methods currently ignore the importance of temporal information between continuously recorded frames, which can easily result in a high false positive rate in the segmentation results.

In this paper, a two-stage system is proposed for real-time guidewire tracking and segmentation, making the following contributions: (1) A bounding box detector for guidewire detection is trained, using the original X-ray images as well as synthetically generated ones, followed by a refinement module based on spatiotemporal constraints to robustly localize the guidewire and suppress false positive detections. (2) A novel efficient network for guidewire segmentation is proposed, which achieves promising performance and strong robustness to low quality X-ray images by incorporating a hessian-based enhancement and attention modules. (3) The whole system is designed to perform in real-time and achieves an inference rate of approximately 35 FPS on a GPU.

2. METHOD

In our work, we propose a two-stage framework for guidewire tracking (see Fig 1), that consists of 1) a temporal-aware detection stage and 2) a hessian-enhanced segmentation stage.

2.1 Guidewire Localization.

In the first stage, YOLOv5s is chosen as the detector to ensure real-time performance of the detector [9], however, we make the following adjustments:

Alg.1: Refinement module to further suppress false positive detection

Input : $Pred_H^t, Pred_L^t, O^{t-1}, \hat{O}^{t-1}, \tau$

- 1 **if** t is 1, **then** $O^t = Pred_H$; $\hat{O}^{t-1} = Pred_L$
- 2 **else**
- 3 $A^{t-1} = O^{t-1}; B^t = Pred_H^t \cup Pred_L^t$
- 4 **if** A^{t-1} is empty, **then** $A^{t-1} = A^{t-1} \cup \hat{O}^{t-1}$, **end if**
- 5 **for** $a_i \in A^{t-1}$, **do** # calculate the IOU score between A^{t-1} and B^t
- 6 $s = \text{box_iou}(a_i, B^t) \cdot (\text{box_iou}(a_i, B^t) > \tau)$
- 7 **if** $\text{sum}(s) > 0$, **then**
- 8 $\text{add } s \times \{B^t\}^T$ into O^t
- 8 **if** a_i in O^{t-1} , **then** delete a_i from O^{t-1}
- 10 **if** s_j in s and $b_j \in B^t$ in $Pred_H^t$, **then** delete b_j from $Pred_H^t$
- 11 $\hat{O}^t = O^{t-1} \cup Pred_H^t$

Return O^t, \hat{O}^t

(1) YOLOv5s only considers spatial but not temporal information. However, due to rather smooth motions we can assume the movement of the guidewire in the image space in consecutive frames too be limited. Therefore, to leverage temporal information we use three consecutive frames as input and introduce a refinement module to further improve the detection precision.

(2) In YOLOv5s, each predicted bounding box is associated with a confidence score and a threshold manually set to obtain the final detection. However, an optimal threshold can be difficult to find and, in addition, easily result in false positives and false negatives in the detection results. To alleviate this issue, instead, the confidence threshold is determined automatically based on the maximum confidence value among all the detection boxes, e.g. $0.001 \cdot \text{maximum confidence value}$.

(3) In our method, the output bounding boxes of YOLOv5s are divided into two lists $Pred_H$ and $Pred_L$ depending on whether a box's confidence score is larger than 0.5, $Pred_H$, or lower, $Pred_L$. Since the position of the guidewire in two consecutive frames should be close, we calculate a matching relationship among the boxes in two consecutive frames by their Intersect over Union (IOU-score). Then, all the boxes, whose IOU-score with the box at timestep $t-1$ is larger than $\tau=0.25$, are merged as refined candidates of the bounding box at timestep t . Finally, the updated boxes are stored in O^t ; the unmatched boxes in O^{t-1} and $Pred_H^t$ are stored in \hat{O}^t . Here, O^t is used to store the bounding boxes already confirmed to contain a guidewire at timestep t ; \hat{O}^t is used to store the bounding boxes temporarily believed to contain a guidewire at timestep t and need to be further confirmed at the next timestep. The complete process of refinement module is shown in Alg.1.

2.2 Guidewire Segmentation.

After the detection stage, the patches that contain the guidewire are cropped based on the detected bounding boxes. Then, we propose HessianNet for guidewire segmentation, which consists of three modules: a hessian layer, an encoder module and decoder module, as shown in the red dotted box in Fig. 1. Input grayscale patches of size 224×224 are first processed by the hessian layer, as shown in Fig. 2, which is used to extract eigenvalue features and improve the quality of the input image. Next, the improved image is fed into the encoder module and the eigenvalue features are concatenated with the features extracted by the first Resnet-block. Maxpooling is then performed in the area of 2×2 with a stride of 2. For the following, each encoder block in the encoder consists of a Resnet-block, a dual self-attention block, which is used to capture the long-range dependency of the features, and a maxpooling layer. Then, the decoder module is employed to integrate the high-level and low level features and recover the resolution of the feature maps from 14×14 to 224×224 . Each decoder block

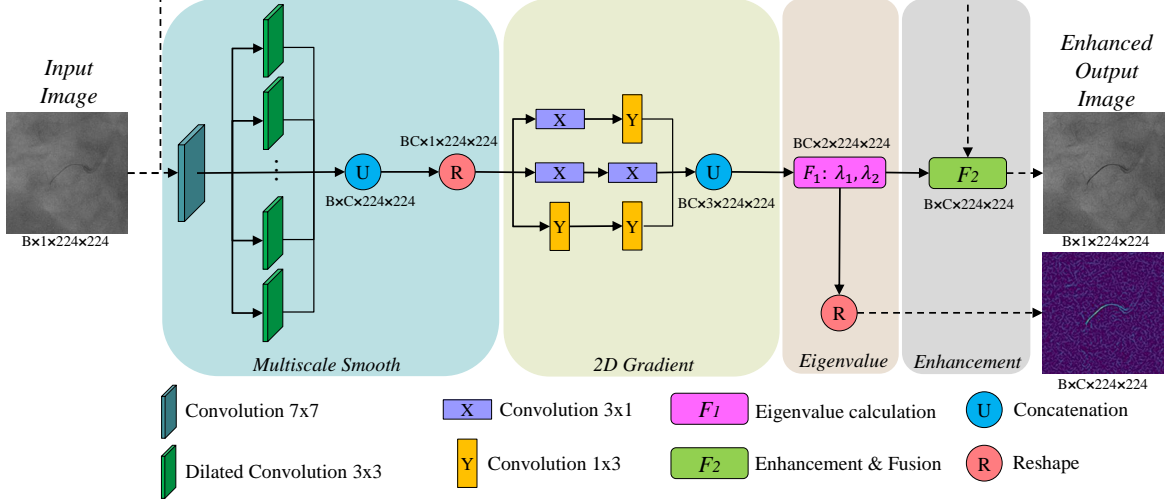


Figure 2. The architecture of the proposed Hessian Layer, which outputs multi-scale eigenvalue features λ_1 and enhances the guidewire in comparison to the original 2D images.

in the decoder consists of a deconvolution, batch normalization, a Resnet-block and a dual self-attention block. Finally, a convolution with a kernel size of 1×1 and a sigmoid function are used to output the segmentation result.

Hessian layer. Within the hessian layer, we reformulate the hessian-based enhancement process as part of the neural network, such that it can be trained with our network architecture. First, a 7×7 convolution and several 3×3 dilated convolution operations are employed to extract multi-scale features, where the weights are initialized using the Gaussian function. Then, a 1×3 1D-convolution and a 3×1 1D-convolution are used to calculate the second-order gradients on each feature map, where the weight of the 1D-convolution is frozen as $[0.5, 0, -0.5]$. Later, the two eigenvalue maps λ_1 and λ_2 of each feature map can be calculated as:

$$\lambda_1(D_{xx}, D_{xy}, D_{yy}) = \frac{(D_{xx} + D_{yy}) - \sqrt{(D_{xx} - D_{yy})^2 + 4D_{xy}^2}}{2} \quad (1)$$

$$\lambda_2(D_{xx}, D_{xy}, D_{yy}) = \frac{(D_{xx} + D_{yy}) + \sqrt{(D_{xx} - D_{yy})^2 + 4D_{xy}^2}}{2} \quad (2)$$

where D_{xx}, D_{xy}, D_{yy} are the second-order gradients. In this work, the enhancement function proposed by [10] is employed to produce the enhancement map. Finally, the input image and enhancement map are fused to improve the contrast of the guidewire. Meanwhile, the eigenvalue feature λ_2 is also stored and later reused to provide preliminary guidelines for guidewire identification.

Dual self-attention block. Note, instead of naively integrating the dual self-attention module at the end of the encoder [11], we employ it at each level of the encoder and decoder. However, the pair-wise attention computation among all pixels is highly inefficient and redundant. For improved efficiency, we first use a max-pooling operation to project the high-dimensional features to low-dimensional space and then calculate the low-rank spatial and channel affinity matrix.

3. EXPERIMENTS

In the following we evaluate our method with respect to both detection as well as segmentation performance and in addition evaluate the robustness of our and state-of-the-art methods with respect to the input image quality.

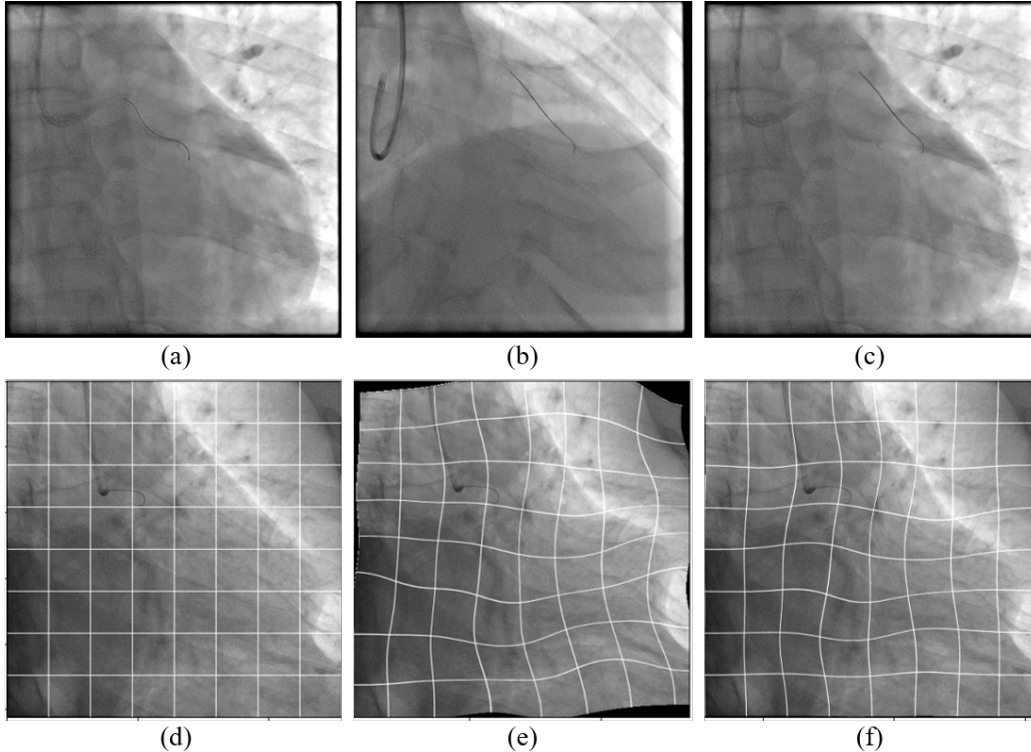


Figure 3. Exemplary synthetic images and elastic deformation. A synthetic image (c) is generated based on source images (a) and (b). A elastic deformed image (e) and a boundary fixed elastic deformed image (f) is generated based on source image (d).

3.1 Dataset

102 sequences from 21 patients are collected from ZhongDa Hospital Southeast University, China, overall containing 5238 X-ray images with a resolution of 512×512 . The images are divided into a training (4112 images from 80 sequences) and testing set (1126 images from 22 sequences). The ground truth of the guidewire in each frame has been annotated by an experienced intervention radiologist.

3.2 Implementation Details.

In this work, the Dice loss is adopted as the objective function for the training of the network. The proposed HessianNet was implemented in the PyTorch library with a NVIDIA GPU (Quadro RTX 6000). Adam optimizer is employed as the overall optimizer where the learning rate is set as 0.0005 initially and decreases using exponential decay with the decay rate of 0.9. The batch size is set to 8, and the network is trained with a maximum number of 100 epochs. For the detection phase, the input image with its origin size of 512×512 is used and for data augmentation, boundary fixed elastic deformations and synthetic image generation is used. For that purpose, the synthetic images are generated by merging the guidewire from one sequence and the background from another X-ray sequence, as shown in Fig. 3. For the segmentation phase, the size of the input image is cropped to 224×224 , and for data augmentation, random horizontal flip, random vertical flip, random rotation $[-90, 90]$, random brightness ratio $[0.8, 1.2]$ and random contrast ratio $[0.8, 1.2]$ are adopted.

3.3 Guidewire Detection.

Here, three simple evaluation metrics are used: to count the number of true positives (TP), false positives (FP) and false negatives (FN) in all frames in the test sequences. TP indicates that the guidewire is completely within

Table 1. Inclusion of temporal information and the detector’s performance. Our refinement step is abbreviated as Ref., Aug. and C3 stand for the inclusion of data augmentation and consecutive frames as input to the detector.

	Yolov5s	Yolov5s Aug.	Yolov5s C3+Aug.	Yolov5s C3+Aug.+Ref.
TP	1082	1109	1112	1125
FN	44	17	14	1
FP	7	2	1	0

Table 2. Performance of our method, HessiaNet, in comparison to the state of the art.

Method	U-Net [13]	R2UNet [14]	ResUnet [15]	FARNet [8]	CSNet [11]	HessianNet w/o Attention	HessianNet w/o Enhance	HessianNet
Dice	0.8890	0.8939	0.8968	0.8981	0.8984	0.8987	0.8984	0.8990
Sensitivity	0.8840	0.8960	0.8908	0.8921	0.8909	0.8954	0.8970	0.8973
FDR	0.0987	0.1030	0.0923	0.1013	0.0897	0.0915	0.0930	0.0947
HD	0.4089	0.3488	0.3225	0.3362	0.3439	0.3123	0.3126	0.3070

Table 3. Performance of our method, on difficult examples, in comparison to the state of the art.

Method	U-Net [13]	R2UNet [14]	ResUnet [15]	FARNet [8]	CSNet [11]	HessianNet w/o Attention	HessianNet w/o Enhance	HessianNet
Dice	0.7592	0.8137	0.8149	0.8198	0.8228	0.8270	0.8260	0.8292
Sensitivity	0.6932	0.7985	0.7767	0.8090	0.7992	0.8113	0.8115	0.8196
FDR	0.1382	0.1610	0.1356	0.1630	0.1417	0.1538	0.1554	0.1571
HD	2.2291	1.0787	0.9019	1.0454	0.7979	0.7116	0.6962	0.65520

the predicted bounding box; FP indicates that there is no guidewire within the predicted bounding box; FN means that the guidewire is not detected or the predicted bounding box cannot cover the guidewire completely.

Table 1 summarizes the performance of our detector where we compare between the original Yolov5s model, the inclusion of 1) data augmentation during training (in the form of elastic deformation and synthetic image generation, i.e. fusing the guidewire of one sequence with the background of another X-ray sequence), 2) three consecutive frames as input to the detector (C3) and 3) the proposed bounding box refinement step. From the Table 1, we can see that the original Yolov5s works well on this task, but there are still some targets missing and some false positive results. Our improved model (i.e. Yolov5s+C3+Aug.+Ref.), in comparison, can significantly reduce the number of missing targets and false positives in the outputs.

3.4 Guidewire Segmentation.

We compare our method to recent state-of-the-art segmentation models using the following metrics: Dice, Sensitivity, False Discovery Rate (FDR), and Hausdorff Distance (HD) [12]. Further, we evaluate the effect of including the proposed hessian layer and dual self-attention block, for which the results are summarized in Table 2. Meanwhile, qualitative examples of our and the baseline methods can be found in Fig 4. From both the quantitative results and the qualitative results, it is clear that our proposed method outperforms other methods.

To further evaluate our methods’ performance in comparison to the baselines, we provide an analysis with respect to the most difficult examples in our dataset. Based on the predicted segmentations of all methods, any image with a HD score larger than 0.1 will be regard as a difficult example. Table 3 summarizes our findings, which further indicates our proposed method is superior to these baseline methods and achieves the state of art.

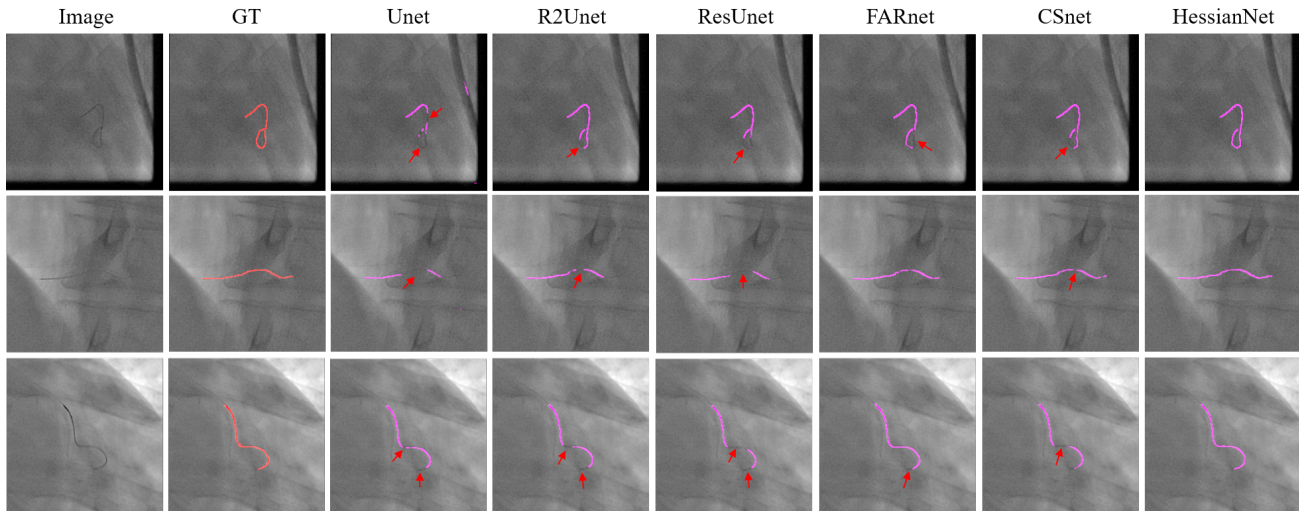


Figure 4. Qualitative results of our and the state-of-the-art methods. Failure cases are highlighted with red arrows.

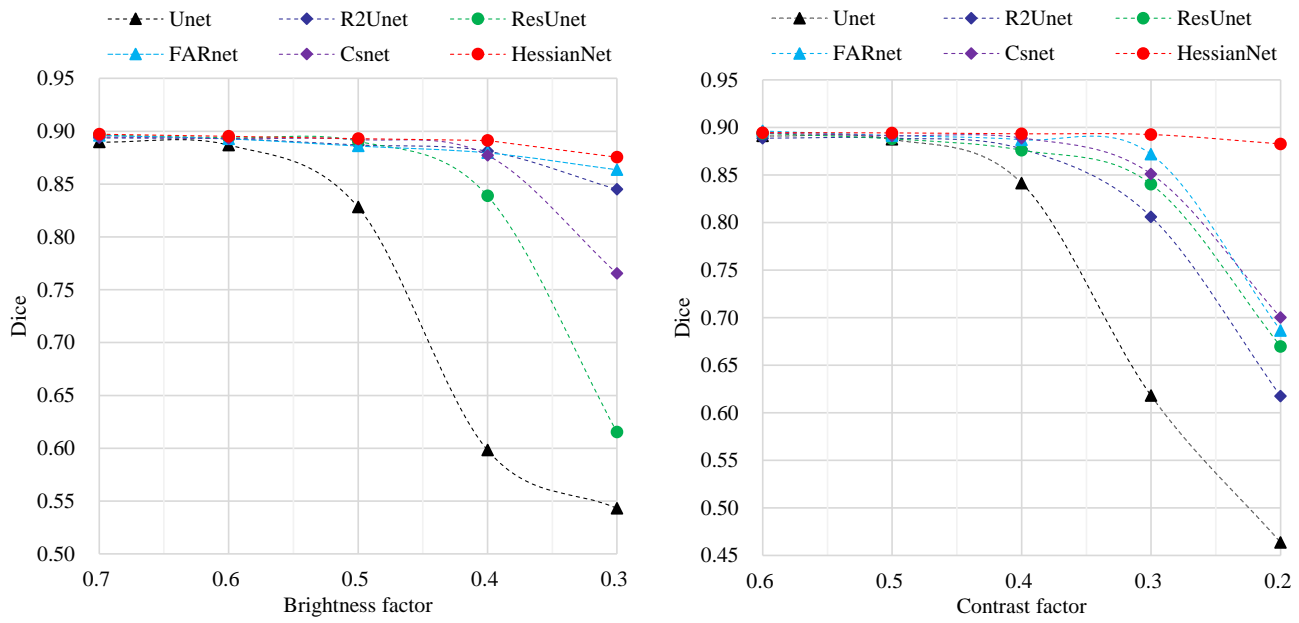


Figure 5. Robustness of our and the baseline methods to variations in image brightness and contrast.

In addition, We analyse the robustness of our and the baseline methods to changes in image brightness and contrast during inference. Fig. 5 summarizes the dice score with respect to varying brightness and contrast ratios and shows that in comparison to our method the baselines are highly susceptible to such changes, resulting in a large drop in dice score.

4. CONCLUSIONS

We propose a two-stage framework for real-time guidewire tracking and segmentation. For the detection phase, an improved detector based on Yolov5s model is trained and a refinement module based on spatiotemporal constraint is proposed to robustly localize the guidewire and suppress false positive detections. For the segmentation phase,

a novel and efficient network which integrates a hessian-based enhancement embedding module and a dual self-attention block is proposed to segment the guidewire from each cropped patch. Quantitative and qualitative evaluation results show that our method outperforms our baselines as well as the current state of the art and has a strong robustness for this task. Moreover, the whole system is designed to perform in real-time and achieves an inference rate of approximately 35 FPS on a NVIDIA GPU (Quadro RTX 6000).

ACKNOWLEDGMENTS

The project was funded by the Bavarian State Ministry of Science and Arts within the framework of the "Digitaler Herz-OP" project under the grant number 1530/891 02 and the China Scholarship Council (File No.202004910390).

References

- [1] Baert, S. A., Viergever, M. A., and Niessen, W. J., "Guide-wire tracking during endovascular interventions," *IEEE Transactions on Medical Imaging* **22**(8), 965–972 (2003).
- [2] Mazomenos, E. B., Chang, P.-L., Rolls, A., Hawkes, D. J., Bicknell, C. D., Poorten, E. V., Riga, C. V., Desjardins, A., and Stoyanov, D., "A survey on the current status and future challenges towards objective skills assessment in endovascular surgery," *Journal of Medical Robotics Research* **1**(03), 1640010 (2016).
- [3] Chen, B.-J., Wu, Z., Sun, S., Zhang, D., and Chen, T., "Guidewire tracking using a novel sequential segment optimization method in interventional x-ray videos," in [2016 IEEE 13th International Symposium on Biomedical Imaging (ISBI)], 103–106, IEEE (2016).
- [4] Vandini, A., Glocker, B., Hamady, M., and Yang, G.-Z., "Robust guidewire tracking under large deformations combining segment-like features (seglets)," *Medical image analysis* **38**, 150–164 (2017).
- [5] Wu, Y.-D., Xie, X.-L., Bian, G.-B., Hou, Z.-G., Cheng, X.-R., Chen, S., Liu, S.-Q., and Wang, Q.-L., "Automatic guidewire tip segmentation in 2d x-ray fluoroscopy using convolution neural networks," in [2018 International Joint Conference on Neural Networks (IJCNN)], 1–7, IEEE (2018).
- [6] Li, R.-Q., Bian, G., Zhou, X., Xie, X., Ni, Z., and Hou, Z., "A two-stage framework for real-time guidewire endpoint localization," in [International Conference on Medical Image Computing and Computer-Assisted Intervention], 357–365, Springer (2019).
- [7] Ambrosini, P., Ruijters, D., Niessen, W. J., Moelker, A., and van Walsum, T., "Fully automatic and real-time catheter segmentation in x-ray fluoroscopy," in [International conference on medical image computing and computer-assisted intervention], 577–585, Springer (2017).
- [8] Zhou, Y.-J., Xie, X.-L., Zhou, X.-H., Liu, S.-Q., Bian, G.-B., and Hou, Z.-G., "A real-time multi-functional framework for guidewire morphological and positional analysis in interventional x-ray fluoroscopy," *IEEE Transactions on Cognitive and Developmental Systems* (2020).
- [9] Jocher, G., Nishimura, K., Mineeva, T., and Vilariño, R., "Yolov5," *Code repository <https://github.com/ultralytics/yolov5>* (2020).
- [10] Jerman, T., Pernuš, F., Likar, B., and Špiclin, Ž., "Enhancement of vascular structures in 3d and 2d angiographic images," *IEEE transactions on medical imaging* **35**(9), 2107–2118 (2016).
- [11] Mou, L., Zhao, Y., Fu, H., Liu, Y., Cheng, J., Zheng, Y., Su, P., Yang, J., Chen, L., Frangi, A. F., et al., "Cs2-net: Deep learning segmentation of curvilinear structures in medical imaging," *Medical image analysis* **67**, 101874 (2021).
- [12] Taha, A. A. and Hanbury, A., "Metrics for evaluating 3d medical image segmentation: analysis, selection, and tool," *BMC medical imaging* **15**(1), 1–28 (2015).
- [13] Ronneberger, O., Fischer, P., and Brox, T., "U-net: Convolutional networks for biomedical image segmentation," in [International Conference on Medical image computing and computer-assisted intervention], 234–241, Springer (2015).
- [14] Alom, M. Z., Hasan, M., Yakopcic, C., Taha, T. M., and Asari, V. K., "Recurrent residual convolutional neural network based on u-net (r2u-net) for medical image segmentation," (2018).
- [15] Zhang, Z., Liu, Q., and Wang, Y., "Road extraction by deep residual u-net," *IEEE Geoscience and Remote Sensing Letters* **15**(5), 749–753 (2018).